Layered Compounds

Deutsche Ausgabe: DOI: 10.1002/ange.201600087
Internationale Ausgabe: DOI: 10.1002/anie.201600087

Decoding the Morphological Diversity in Two Dimensional Crystalline Porous Polymers by Core Planarity Modulation

*Arjun Halder[+], Sharath Kandambeth[+], Bishnu P. Biswal[+], Gagandeep Kaur, Neha Chaki Roy, Matthew Addicoat, Jagadish K. Salunke, Subhrashis Banerjee, Kumar Vanka, Thomas Heine, Sandeep Verma, and Rahul Banerjee**

Abstract: *Two new chemically stable triazine- and phenyl-core-based crystalline porous polymers (CPPs) have been synthesized using a single-step template-free solvothermal route. Unique morphological diversities were observed for these CPPs [2,3-DhaTta (ribbon) and 2,3-DhaTab (hollow sphere)] by simply altering the linker planarity. A detailed time-dependent study established a significant correlation between the molecular level structures of building blocks with the morphology of CPPs. Moreover, a DFT study was done for calculating the interlayer stacking energy, which revealed that the extent of stacking efficiency is responsible for governing the morphological diversity in these CPPs.*

Two dimensional crystalline porous polymers (CPPs), including covalent organic frameworks (COFs)[1] and covalent triazine frameworks (CTFs),[2] are porous materials constructed by covalently linked light elements, such as C, N, O, H, B, and Si. These materials have triggered substantial research interest because of their extensive applications in molecular storage,[3] catalysis,[4] sensing,[5] and opto-electronics.[6] However, the overall properties of such porous materials do not rely only on their composition, structure, and porosity, but also on their nanoscale morphologies.[7] Therefore, an explicit understanding of the morphology-modulation with respect to their constituents is required.[8] To achieve such a molecular level understanding, herein we report two CPPs that self-assemble to ribbon and hollow spherical[9] morphologies upon crystallization in a single step without any templating agents. Hollow spherical structures are considered to be a highly important morphology in polymeric materials owing to several potential applications. However, their existence is extremely rare and often require the usage of templating agents.[10] The intermediates responsible for producing these above morphologies were prepared at different time intervals to understand the mechanism for the formation of the final morphology (at 72 h).

The CPPs reported here show high crystallinity as revealed from their PXRD patterns (Figure 1). A high intense peak at 2.8° (2θ) for 2,3-DhaTta and 2,3-DhaTab (Figure 1e and 1f, respectively) appear owing to the strong reflections from the 100 planes. 2,3-DhaTta and 2,3-DhaTab show other minor peaks at 4.9, 5.7, 7.5, and 9.9° (2θ) owing to the reflections from the 110, 200, 120, and 220 planes, respectively. Peaks at 26° (2,3-DhaTta) and 25.8° (2,3-DhaTab) correspond to their 001 plane reflections. The d-spacing values between the 001 planes were used to calculate the π-π stacking distances between vertically stacked CPP layers [3.3 Å and 3.4 Å in the respected CPPs]. The high crystallinity of these CPPs is attributed to the presence of strong intramolecular O–H···N hydrogen bonding[11] interactions between the imine nitrogen and the hydroxy functionality of the aldehyde core, which is influential in keeping the phenyl rings in one plane and increases stacking interactions within adjacent CPP layers. To get an overview of the hydrogen bonding effect on the CPP backbone, we crystallized three reference compounds, SaTta, 2,3-Dha-ani,[12] and SaTab[9] (Figure 1b–d). X-ray single-crystal structure analysis showed that the three phenyl rings connected to the central triazine core in SaTta are almost in the same plane (torsion angles are 174.7, 176.3, and 179.9°; Supporting Information), whereas for SaTab, the central triphenyl cores are not in the same plane (torsion angles are 145.5, 149.6, and 154.5°) to avoid steric interactions among the *ortho* hydrogens. On the other hand, in 2,3-Dha-ani, the central benzene ring of the respective aldehyde counterparts are out of plane (torsion angles are 134.5 and 135.9°). Interestingly, the structural features of these reference compounds largely depended upon the intramolecular O–H···N hydrogen bonding [SaTta $D = 2.63$ Å, $d = 1.98$ Å, $\theta = 141.6°$; SaTab 2.61 Å, 1.88 Å, 146.6°; and 2,3-Dha-ani 2.59 Å, 1.86 Å, 146.6°, respectively].

[*] A. Halder,[+] S. Kandambeth,[+] B. P. Biswal,[+] S. Banerjee, Prof. Dr. K. Vanka, Prof. Dr. R. Banerjee
Academy of Scientific and Innovative Research (AcSIR)
Physical/Materials Chemistry Division
CSIR-National Chemical Laboratory
Dr. Homi Bhabha Road, Pune-411008 (India)
E-mail: r.banerjee@ncl.res.in

J. K. Salunke
Polymer Science and Engineering Division
CSIR-National Chemical Laboratory
Dr. Homi Bhabha Road, Pune 411008 (India)

G. Kaur, Prof. Dr. S. Verma
DST-Thematic Unit of Excellence on Soft Nanofabrication
Indian Institute of Technology Kanpur
Kanpur-208016 (India)

N. C. Roy
Centre for Research in Nanotechnology and Science
Indian Institute of Technology Bombay
Mumbai-400076 (India)

Dr. M. Addicoat, Prof. Dr. T. Heine
Center for Functional Nanomaterials
School of Engineering and Science
Jacobs University Bremen, Research III, Room 61
Campus Ring 1, 28759 Bremen (Germany)

[+] These authors contributed equally to this work.

Supporting information for this article can be found under: http://dx.doi.org/10.1002/anie.201600087.

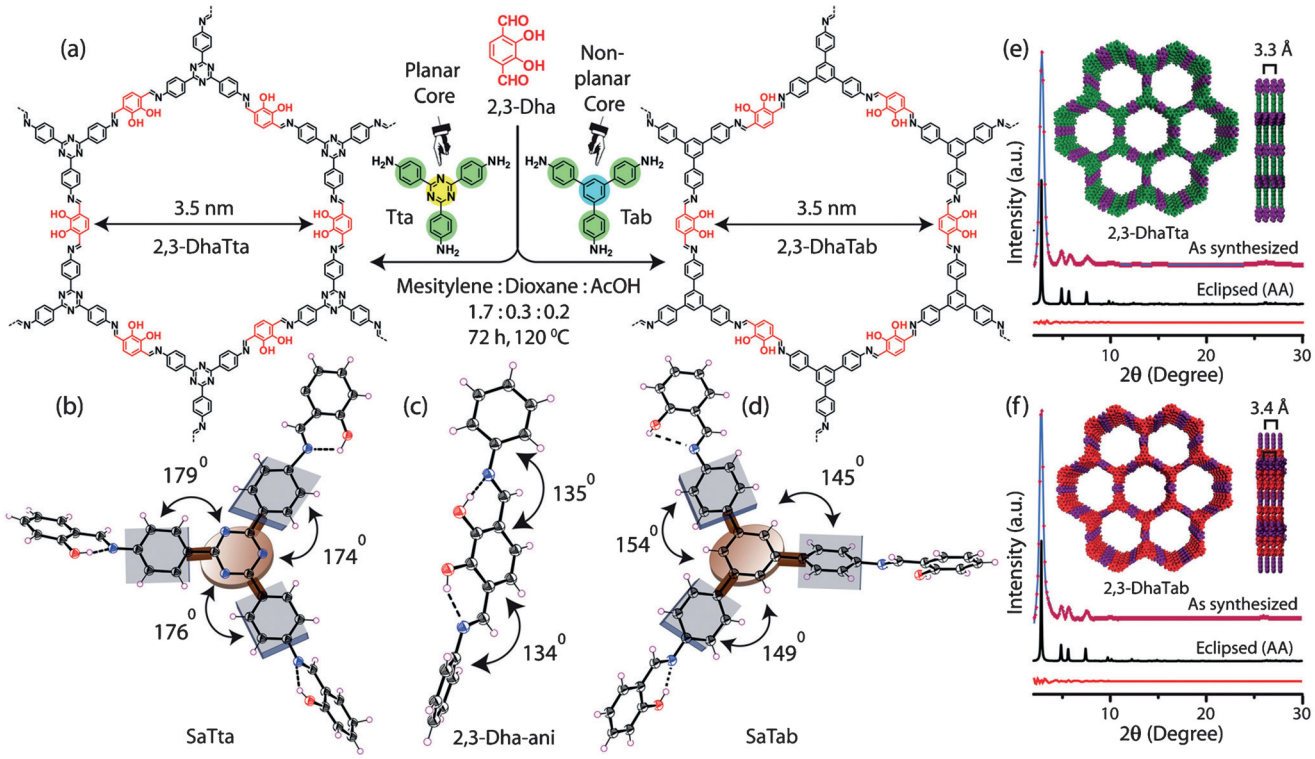

Figure 1. a) Synthesis of 2,3-DhaTta and 2,3-DhaTab. The ORTEP diagram of the reference compounds b) SaTta, c) 2,3-Dha-ani, and d) SaTab [carbon (black), nitrogen (blue), hydrogen (pink) and oxygen (red)] were synthesized from their respective aldehydes and amines. The experimental PXRD patterns (blue) compared with the simulated (eclipsed; black) and Pawley refined difference (red) [e) Rp = 4.6%, Rwp = 2.3% and Rwp (w/o bck) = 2.2% for 2,3-DhaTta and f) Rp = 7.1%, Rwp = 3.6% and Rwp (w/o bck) = 3.7% for 2,3-DhaTab].

These observations clearly indicate that 2,3-DhaTta should exhibit a more planar structure compared to 2,3-DhaTab. The experimental PXRD patterns match well with the simulated slipped-AA stacking model for these two CPPs (Figures S4 and S5). The model structure matches well with the space group triclinic *P*1 in both of the CPPs. To elucidate the unit cell parameters, Pawley refinement was performed, which indicated good agreement between the simulated and experimental PXRD patterns. The unit cell parameters for the CPPs 2,3-DhaTta and 2,3-DhaTab appeared as $a = 37.1$, $b = 37.1$, $c = 3.5$ and $a = 37.3$, $b = 37.3$, $c = 3.5$ respectively (Supporting Information).

FT-IR analysis for the CPPs reported here showed the complete disappearance of the primary −N−H stretching band (3200–3460 cm^{-1}) of the parent amines as well as the −C=O stretching frequency of around 1660 cm^{-1} for aldehydes used in the synthesis (Supporting Information). Moderate and strong bands, respectively for triazine- and phenyl-core-based CPPs, appeared around 1616 cm^{-1}, and reflect the formation of −C=N linkages similar to those found in the reference compounds (SaTta and SaTab). The solid-state ^{13}C NMR spectra of 2,3-DhaTta exhibited a strong signal at ≈166.5 ppm originating from the triazine core carbon atoms only, as this peak is completely absent in 2,3-DhaTab. The signal at around ≈157.6 ppm was assigned to the imine linkage carbon atoms present in both CPPs (Figure S12). The CPPs followed the type IV reversible N_2 adsorption isotherm, which reflects their mesoporous nature (Supporting Information). The Brunauer–Emmett–Teller (BET) surface areas of 2,3-DhaTta and 2,3-DhaTab were found to be 1700 and 413 $m^2 g^{-1}$ respectively. The high surface area of 2,3-DhaTta compared to 2,3-DhaTab could be due to its high crystallinity and exposed pore structure, which may originate from strong π-π stacking interactions between the layers (that is, a more planar structure). Planarity and stacking interactions between the vertically stacked layers decreases, which is reflected in the lower surface area in 2,3-DhaTab. The experimental pore widths of 2,3-DhaTta and 2,3-DhaTab were calculated to be 3.5 nm (Figure S14). The TGA profile shows that the CPPs are thermally stable up to 350 °C (Figure S12). The CPP samples were treated with water, 3 M HCl, and 3 M NaOH to ensure their chemical stability. After 3 days treatment in water and acid, retention of the PXRD pattern along with no changes in the FTIR spectra (Supporting Information) indicated their stability in water and in 3 M HCl. The N_2 adsorption isotherm showed that these CPPs are still porous after prolonged water treatment. The CPPs were found to be unstable in 3 M NaOH after 3 days.

In 2,3-DhaTta, ribbon-shaped crystallites (length around 200 nm) have been found from TEM (Figure 2e, 12 h; Supporting Information, Figure S22). On the other hand, SEM and TEM images show that 2,3-DhaTab forms hollow spheres that are interconnected through their mesoporous walls (Figure 2k,l; Supporting Information, Figures S19 and S21). The spherical nature of 2,3-DhaTab (diameter around 400 nm) was confirmed by AFM analysis (Figure S23). We tried to establish a correlation between the crystallite morphology and its molecular level structure based on

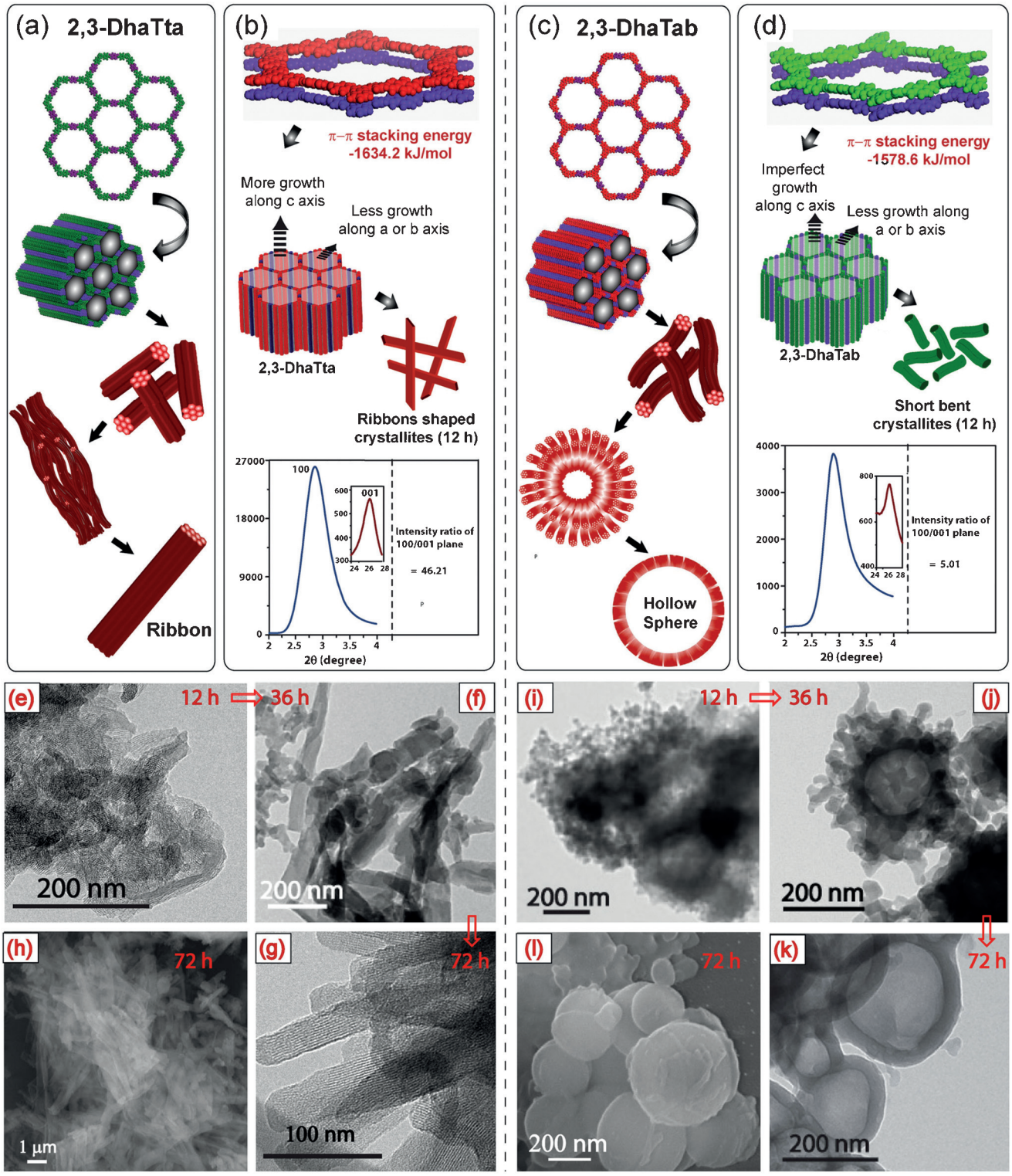

Figure 2. The mechanism of the formation of ribbon (a) and hollow sphere (c) for CPP 2,3-DhaTta, and 2,3-DhaTab, respectively. TEM images of CPPs recorded at different time intervals and SEM images (bottom; 72 h, time shown in red) for a and c. (b and d) Expected growth mechanism of respective CPP crystallites at 12 h, the stacking model along with stacking energy value (from DFT) mentioned for two adjacent hexagonal CPP layers; PXRD pattern (of 12 h sample) along with intensity ratio of 100 to 001 planes shown for each CPP.

microscopy images. The structure of 2,3-DhaTta could be defragmented into two reference compounds SaTta and 2,3-Dha-ani. The reference compound SaTta showed three nearly planar phenyl rings with respect to the triazine core, whereas the phenyl rings from the aldehyde part (between two *cis* imine linkages) in 2,3-Dha-ani were slightly out of plane (Figure 1b and c). Moreover, the π-π stacking energy per hexagon was calculated to determine the stacking efficiency

among the vertically stacked CPP layers, and it was found to be $-1634.2\ kJ\,mole^{-1}$ in 2,3-DhaTta (Figure S24). Interestingly, the PXRD intensity ratio between the 100 to the 001 plane of the sample retrieved after 12 h of reaction was 46.2 (Figure 2b). This high value directly indicated that each individual layer utilizes the strong π-π stacking interaction to interact with other layers to extend along the *Z* direction compared to *X* and *Y* directions (Figure S26). Thus, the growth continues to form ribbons (Figure 2e). These crystallites self-aggregate into larger ribbon-shaped crystallites after 36 h (length ca. 515 nm, width ca. 90 nm; Figure 2f). Finally, this ribbon-like morphology is prominently visible at 72 h by SEM and TEM (Figure 2g,h; Supporting Information, Figures S18 and S20). As observed by SEM and TEM, 2,3-DhaTab has a hollow spherical morphology after 72 h (Figure 2k,l; Supporting Information, Figures S19 and S21). TEM images clearly showed that at the beginning of the reaction, mostly small bent fibers (length ca. 25–55 nm) were formed (Figure 2i; Supporting Information, Figure S22). We tried to gain a greater understanding from their molecular level structure and PXRD (Figure 2d). The central four phenyl rings (one core phenyl and three outer phenyls from the amine counterpart) are completely out of plane with respect to each other (SaTab; Figure 1d) and the benzene core, connected between two *cis* imine bonds, were not in the same plane (2,3-Dha-ani; Figure 1c), which means that the π-π stacking interaction in this case is imperfect as the layers are extremely non-planar (ca. π-π stacking energy $-1578.7\ kJ\,mole^{-1}$ from DFT; Figure S25). This imperfect stacking hinders the growth of CPP fibers along the *Z* axis. PXRD intensity ratio between 100 to 001 planes is 5 (Figure 2d), which is 9-times smaller compared to the PXRD intensity ratio between 100 to 001 planes in 2,3-DhaTta. This indicates that the growth along the *Z* direction is absolutely minimal. From the TEM images, it was seen that the fibers were bent, which could be due to improper stacking between the layers and further self-aggregates to give a dense spherical morphology as time progresses (Figure 2i). However, with time, the crystallites gradually diffuse from the center of the dense sphere to its wall, making a hollow interior inside between 36–48 h (Figure 2j; Supporting Information, Figure S27). At 72 h, an entirely dark wall with a bright contrast inside of the sphere (wall thickness ca. 25–50 nm and diameter ca. 100–500 nm) was found to form, as revealed by TEM, which reflects a hollow spherical nature (Figure 2k ; Supporting Information, Figure S21). It is noteworthy that higher curvature is associated with a higher surface free energy.[14] The formation of a hollow sphere in this case is influenced by mass diffusion from the interior, where the particles are less compact and experience higher surface free energy, to the exterior, in order to reduce their surface free energy. Based on the above observations, we believe that the overall morphological evolution in 2,3-DhaTab is governed by the Ostwald ripening process (Figure S27).[13]

In summary, we have designed and successfully synthesized two new imine-linked chemically stable, crystalline, porous, morphologically diverse polymers. The presence of strong intramolecular H-bonding forces a stiff and planar CPP structure, which is the basis of the high surface area and crystallinity. These CPPs display different morphologies, such as ribbons and spheres, as observed from SEM and TEM imaging. In the case of triazine-based CPP (2,3-DhaTta) the crystallite self-assembles to ribbons. However, in the phenyl-core-based CPP (2,3-DhaTab) the morphology dramatically reshapes to hollow spheres through an inside-out Ostwald ripening mechanism. A thorough DFT study was carried out to validate the experimental results. From that, it was confirmed that the extent of π-π stacking efficiency among the 2D CPP layers is accountable for their morphological diversity along with a dramatic change of surface area. We believe that a detailed investigation of diversity in the self-assembly process, along with valuable morphologies, will open up a new domain of exciting research area in CPPs.

Acknowledgements

A.H. and S.K. acknowledge CSIR, and B.P.B. acknowledges UGC, India for a research fellowship. R.B. acknowledges CSIR's XII[th] Five Year Plan Project (CSC0122 and CSC0102) for funding. Financial assistance from DST (SB/S1/IC-32/2013), DST Indo-Singapore (INT/SIN/P-05) and DST Nano-mission (SR/NM/NS-1179/2012G) are acknowledged. We acknowledge Dr. T. G. Ajithkumar and S. B. Nair for the NMR facility; Dr. K. Guruswamy for the PXRD facility; S. Bera, D. B. Shinde for SCXRD data collection. We acknowledge Prof. R. Rao, IIT Bombay and the support of Center for Advance Imaging, IIT Kanpur, for SEM and TEM experiments and image acquisition. We acknowledge Dr. P. P. Wadgaonkar, CSIR-NCL for valuable discussions.

Keywords: covalent organic frameworks · density functional calculations · dihedral angles · morphology · stacking interactions

How to cite: *Angew. Chem. Int. Ed.* **2016**, *55*, 7806–7810
Angew. Chem. **2016**, *128*, 7937–7941

[1] a) A. P. Côté, A. I. Benin, N. W. Ockwig, A. J. Matzger, M. O'Keeffe, O. M. Yaghi, *Science* 2005, 310, 1166; b) J. R. Hunt, C. J. Doonan, J. D. LeVangie, A. P. Cote, O. M. Yaghi, *J. Am. Chem. Soc.* 2008, 130, 11872; c) F. J. Uribe-Romo, C. J. Doonan, H. Furukawa, K. Oisaki, O. M. Yaghi, *J. Am. Chem. Soc.* 2011, 133, 11478; d) E. L. Spitler, W. R. Dichtel, *Nat. Chem.* 2010, 2, 672; e) X. Chen, M. Addicoat, E. Jin, L. Zhai, H. Xu, N. Huang, Z. Guo, L. Liu, S. Irle, D. Jiang, *J. Am. Chem. Soc.* 2015, 137, 3241; f) R. W. Tilford, W. R. Gemmill, H. C. Zur Loye, J. J. Lavigne, *Chem. Mater.* 2006, 18, 5296.

[2] a) L. Stegbauer, K. Schwinghammer, B. V. Lotsch, *Chem. Sci.* 2014, 5, 2789; b) V. S. Vyas, F. Haase, L. Stegbauer, G. Savasci, F. Podjaski, C. Ochsenfeld, B. V. Lotsch, *Nat. Commun.* 2015, 6, 8508; c) L. Hao, J. Ning, B. Luo, B. Wang, Y. Zhang, Z. Tang, J. Yang, A. Thomas, L. J. Zhi, *J. Am. Chem. Soc.* 2015, 137, 219; d) P. Katekomol, J. Roeser, M. J. Bojdys, J. Weberund, A. Thomas, *Chem. Mater.* 2013, 25, 1542.

[3] a) C. J. Doonan, D. J. Tranchemontagne, T. G. Glover, J. R. Hunt, O. M. Yaghi, *Nat. Chem.* 2010, 2, 235; b) M. Dogru, M. Handloser, F. Auras, T. Kunz, D. Medina, A. Hartschuh, P. Knochel, T. Bein, *Angew. Chem. Int. Ed.* 2013, 52, 2920; *Angew. Chem.* 2013, 125, 2992; c) C. R. DeBlase, K. E. Silberstein, T. T. Truong, H. D. Abruña, W. R. Dichtel, *J. Am. Chem. Soc.* 2013,

135, 16821; d) S. Y. Ding, J. Gao, Q. Wang, Y. Zhang, W. G. Song, C. Y. Su, W. Wang, *J. Am. Chem. Soc.* 2011, 133, 19816.
[4] a) H. Xu, J. Gao, D. Jiang, *Nat. Chem.* 2015, 7, 905; b) P. Pachfule, S. Kandambeth, D. D. Díaz, R. Banerjee, *Chem. Commun.* 2014, 50, 3169; c) M. G. Rabbani, A. K. Sekizkardes, Z. Kahveci, T. E. Reich, R. Ding, H. M. El-Kaderi, *Chem. Eur. J.* 2013, 19, 3324.
[5] a) G. Das, B. P. Biswal, S. Kandambeth, V. Venkatesh, G. Kaur, M. Addicoat, T. Heine, S. Verma, R. Banerjee, *Chem. Sci.* 2015, 6, 3931; b) S. Wan, J. Guo, J. Kim, H. Ihee, D. Jiang, *Angew. Chem. Int. Ed.* 2008, 47, 8826; *Angew. Chem.* 2008, 120, 8958.
[6] D. Gopalakrishnan, W. R. Dichtel, *J. Am. Chem. Soc.* 2013, 135, 8357.
[7] a) J. S. Chen, L. A. Archer, X. W. Lou, *J. Mater. Chem.* 2011, 21, 9912; b) M. A. Mahmoud, R. Narayanan, M. A. El-Sayed, *Acc. Chem. Res.* 2013, 46, 1795.
[8] a) J. Lee, K. Baek, M. Kim, G. Yun, Y. H. Ko, N. S. Lee, I. Hwang, J. Kim, R. Natarajan, C. G. Park, W. Sung, K. Kim, *Nat. Chem.* 2014, 6, 97; b) K. Baek, G. Yun, Y. Kim, D. Kim, R. Hota, I. Hwang, D. Xu, Y. H. Ko, G. H. Gu, J. H. Suh, C. G. Park, B. J. Sung, K. Kim, *J. Am. Chem. Soc.* 2013, 135, 6523.
[9] a) S. Kandambeth, V. Venkatesh, D. B. Shinde, S. Kumari, A. Halder, S. Verma, R. Banerjee, *Nat. Commun.* 2015, 6, 6786; b) K. B. Joshi, S. Verma, *Angew. Chem. Int. Ed.* 2008, 47, 2860; *Angew. Chem.* 2008, 120, 2902.
[10] a) B. Wang, J. S. Chen, H. B. Wu, Z. Wang, X. W. Lou, *J. Am. Chem. Soc.* 2011, 133, 17146; b) C. A. Wang, S. Li, L. An, *Chem. Commun.* 2013, 49, 7427; c) L. Hua, Q. Chen, *Nanoscale* 2014, 6, 1236; d) Y. Zhu, J. Shi, W. Shen, X. Dong, J. Feng, M. Ruan, Y. Li, *Angew. Chem. Int. Ed.* 2005, 44, 5083; *Angew. Chem.* 2005, 117, 5213.
[11] a) G. R. Desiraju, T. Steiner, *The Weak Hydrogen Bond in Structural Chemistry and Biology*, Oxford University Press, Oxford, 1999; b) G. R. Desiraju, *Acc. Chem. Res.* 2002, 35, 565.
[12] D. B. Shinde, S. Kandambeth, P. Pachfule, R. R. Kumar, R. Banerjee, *Chem. Commun.* 2015, 51, 310.
[13] a) J. Hu, M. Chen, X. S. Fang, L. M. Wu, *Chem. Soc. Rev.* 2011, 40, 5472; b) J. Li, H. Zeng, *J. Am. Chem. Soc.* 2007, 129, 15839; c) J. Huo, L. Wang, E. Irran, H. Yu, J. Gao, D. Fan, B. Li, J. Wang, W. Ding, A. M. Amin, C. Li, L. Ma, *Angew. Chem. Int. Ed.* 2010, 49, 9237; *Angew. Chem.* 2010, 122, 9423.
[14] a) X. W. Lou, L. A. Archer, Z. C. Yang, *Adv. Mater.* 2008, 20, 3987.

Received: January 5, 2016
Revised: February 5, 2016
Published online: March 8, 2016

